

End-Group-Dominated Molecular Order in Self-Assembled Monolayers

H. Wolf and H. Ringsdorf

Institut für Organische Chemie, Johannes-Gutenberg-Universität, D-55099 Mainz, Germany

E. Delamarche, T. Takami, H. Kang, B. Michel,* and Ch. Gerber

IBM Research Division, Zurich Research Laboratory, CH-8803 Rüschlikon, Switzerland

M. Jaschke, H.-J. Butt, and E. Bamberg

Max-Planck-Institut für Biophysik, Kennedyallee 70, D-60596 Frankfurt/Main, Germany

Received: January 6, 1995[⊗]

Self-assembled monolayers of 6-[4-(phenylazo)phenoxy]hexane-1-thiol (“azobenzene”) on gold have been studied with atomic force microscopy in ethanol and with scanning tunneling microscopy at high gap impedance in air. These azobenzene-functionalized self-assembled monolayers show two stable rectangular lattices having equal dimensions of 0.61 and 0.79 nm and an angle of 89°. We conclude that the lattices are end-group dominated because they are incommensurate with Au(111), they extend over terrace edges with no phase shift, and they can also be observed on polycrystalline gold. The unit cells are populated with two molecules that have aromatic interactions and expose the upper phenyl ring edge of the azobenzene moiety to the surface. The anisotropic electronic shape of these phenyl rings allows distinct, isoenergetic geometries created by laterally shifting and tilting pairs of phenyl rings. The upper edge of these phenyl rings appears to be elliptical in STM images.

1. Introduction

The modification of solid surfaces by spontaneously self-assembling monolayers is a model system for the study of biomembranes and is of technical interest for the fabrication of sensors, transducers, protective layers, and patternable materials (for an overview see refs 1–4). Self-assembled monolayers (SAMs) are formed at a solid–liquid interface by molecules that have a terminal anchoring group with a strong affinity to the solid surface and a long linear alkyl chain that provides upright ordering on the surface.^{5,6} The affinity to the solid surface is provided by a covalent chemical reaction, as in silanes on silicon dioxide,^{5,7,8} by an ionic interaction, as in carboxylic acids on aluminum,⁹ or by a charge-transfer complex, as in alkyl thiols on noble metals.^{10–12} Alkanethiols are the most intensively studied system because they react with several metals that are inert to almost any other reaction. This allows a wide variety of functional groups to be placed at the opposite end of the alkyl chain (ω -functional group).¹³ The functionality of the surface can be used for the formation of multilayers and for the study of recognition reactions at ordered layers.^{14–16} Scanning tunneling microscopy (STM) and atomic force microscopy (AFM) studies showed hexagonal ($\sqrt{3} \times \sqrt{3}$)R30° lattices for unfunctionalized^{17–21} as well as for functionalized thiols on gold.²² High gap impedance STM measurements clearly resolved molecular features such as domain boundaries and superstructures.^{23–25} Recent results for thermally annealed alkanethiols showed that some rows of molecules are missing²⁶ and that the interaction between tails can compensate for these missing lines.²⁷ Simulations and infrared experiments suggest that bulky aromatic units within an alkyl thiol monolayer can change the packing density and the lattice parameters.^{28–30} Aromatic residues are interesting because their behavior in Langmuir–Blodgett (LB) films proves the dominant effect of

the anisotropic interaction on the two-dimensional order.² X-ray diffraction and AFM studies of crystals of polycyclic aromatic molecules show in many cases edge-to-plane interactions between molecules or pairs of molecules in the unit cell.^{31,32} The electronic and thermal properties of azobenzenes make them important constituents of liquid crystals and donor–acceptor bridge systems² and have triggered numerous studies in such fields as nonlinear optics (NLO) and photoisomerization. Azobenzenes as functional groups on SAMs are of particular interest in local probe studies because they affect the electronic properties as well as the lateral packing of the molecules. Their effect on the monolayer structure is investigated using scanning probe microscopies and in addition real-space observation of intermolecular aromatic interaction will be presented.

2. Experimental Section

2.1. Synthesis of 6-[4-(Phenylazo)phenoxy]hexane-1-thiol (Chart 1) (“azobenzene”). The synthesis was carried out in three steps. First the alkyl chain was reacted onto the 4-(phenylazo)phenol via the formation of an ether. Then, the remaining bromo function was converted into the Bunte salt and finally hydrolyzed to the thiol.

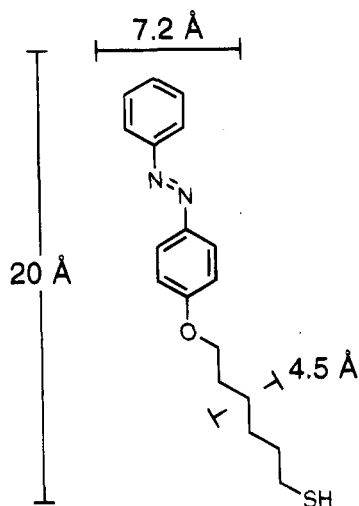
2.1.1. [4-[(6-Bromohexyl)oxy]phenyl]phenyldiazene. A 19.8 g (0.1 mol) amount of 4-(phenylazo)phenol and 122 g (0.5 mol) of 1,6-dibromohexane together with 10 g of potassium carbonate and 0.5 g of potassium iodide were refluxed in 200 mL of pentanone-2 for 1 day. The reaction mixture was filtered while still hot, and the solid was washed with chloroform. Solvent and excess dibromide were distilled from the product. The crude [4-[(6-bromohexyl)oxy]phenyl]phenyldiazene was recrystallized twice from acetone. Yield: 30.3 g (84%).

2.1.2. Bunte Salt. A 1 g (2.8 mmol) amount of [4-[(6-bromohexyl)oxy]phenyl]phenyldiazene was dissolved in 10 mL of ethanol, and 0.75 g (3.0 mmol) of sodium thiosulfate pentahydrate dissolved in 3 mL of water was added. The

* Corresponding author, bmi@zurich.ibm.com.

[⊗] Abstract published in *Advance ACS Abstracts*, April 1, 1995.

CHART 1: Skeleton of the 6-[4-(Phenylazo)phenoxy]hexane-1-thiol Molecule (Whose Full Name Is Abbreviated by the Term "Azobenzene"). Estimated Height of the Molecule and van der Waals Diameters of the Alkyl Chain and of the Azobenzene Group Are Indicated



mixture was refluxed for 2 h. Upon cooling, the Bunte salt precipitated. Yield: 1.09 g (93%).

2.1.3. 6-[4-(Phenylazo)phenoxy]hexane-1-thiol. A 20 mL amount of chloroform and 20 mL of 1M HCl were degassed with nitrogen. Then, 1 g of the Bunte salt was added and the mixture was refluxed for 2 h. After cooling to room temperature, the organic phase was separated, and the aqueous phase was extracted with chloroform. The organic fractions were evaporated to dryness, and the crude 6-[4-(phenylazo)phenoxy]hexane-1-thiol was recrystallized from hexane/acetone 1:1. Yield: 560 mg (74%), mp 79 °C. $^1\text{H NMR}$ (CDCl_3): δ (ppm) 1.35 (t, 1 H, SH), 1.4–1.9 (m, 8 H, aliphatic CH_2), 2.56 (d t, 2 H, SCH_2), 4.05 (t, 2 H, OCH_2), 7.0–7.9 (m, 9 H, aromatic H). Anal. Calcd for $\text{C}_{18}\text{H}_{22}\text{N}_2\text{OS}$ (314.45): C, 68.75; H, 7.05; N, 8.90; S, 10.18. Measd: C, 69.03; H, 7.11; N, 9.03; S, 10.53.

2.2. Substrate and Monolayer Preparation. Au(111) substrates were produced by evaporating 200 nm of gold onto cleaved mica surfaces heated to 340 °C at a pressure of 5×10^{-7} Torr and a rate of 0.5 nm/s.³³ Equivalent substrates were produced with a 20-nm gold layer evaporated onto glow-discharge quartz glass by flame annealing at 700 °C during 30 s and subsequent quenching in methanol.³⁴ Azobenzene thiols were adsorbed from 5×10^{-4} molar solutions in ethanol or dichloromethane. The monolayers had the same properties regardless of which solvent had been used to produce the adsorption. Adsorption times were varied from 2 to 80 h, but showed no difference in the monolayer quality. In contrast to dodecanethiol,²⁴ adsorption at elevated temperature (50 °C) did not increase the average domain size (based on AFM and STM results).

2.3. Characterization of Monolayers. Ellipsometry measurements were taken with an L-115-B Gaertner Scientific Corporation (Chicago) type automatic thin-film ellipsometer operating at 632.8 nm (He–Ne laser) and an angle of incidence of 70°. The polarizer was set at 45°. To determine the thickness of the azobenzene SAM, we first determined the complex refractive index of the gold substrate: $N_s = n_s + k_s i$. As the refractive index varied slightly from substrate to substrate, thickness measurements of the SAMs were performed at the precise locations where n_s and k_s had been measured. As the refractive index (n_f) and thickness of thin films (<5 nm) cannot be determined simultaneously, n_f was set to 1.45. For al-

kanethiols, n_f values are usually between 1.45 and 1.50. An 0.05 increase of n_f induces a 0.1-nm decrease of the calculated thickness.³⁵ The method we used has an accuracy of ± 0.2 nm.

Contact angles were determined at ambient laboratory conditions on a Krüss contact angle goniometer with Millipore water as probe liquid. A microsyringe was used to change the volume of the sessile drop until the front was seen to advance or recede across the surface. Once the observable motion had ceased, the contact angle was measured without removing the needle from the drop.³⁶

2.4. Local Probe Instrumentation and Data Evaluation. STM experiments were carried out under ambient conditions using mechanically cut Pt–Ir tips with an instrument equipped for high-bandwidth measurements at large gap impedance.³⁷ STM scanners were calibrated laterally with Au(111) and graphite and vertically using Au(111) steps. Calibrations were verified under high gap impedance conditions on a superlattice formed by dodecanethiol on Au(111).²⁴ The molecular resolution in the constant-current mode was optimal, having a bias voltage of 0.8–1.0 V (sample positive) and a tunneling current of <1.5 pA. The scanning lines were repeated (2 to 8 times) and averaged to improve the image quality for small scans of a few nanometers in size.

AFM images were taken with a Nanoscope III (Digital Instruments, Santa Barbara, CA) in contact, constant force and friction mode, using sharpened silicon nitride cantilevers (Olympus, Tokyo) 100 μm in length and having a spring constant of 0.092 N/m. AFM scanners were calibrated on mica, and scans were performed in ethanol to prevent surface contamination and to reduce the attractive force between the tip and the sample. The applied forces ranged between 1 and 3 nN without significant influence on the lattice constant. Lattice vectors were calculated using two-dimensional Fourier transforms. To compensate for instrument drift, corresponding vectors from subsequent up and down scans were averaged. Several independent scans on various samples were averaged in reciprocal space after principal lattice vectors were aligned by rotation. Optimal alignment was confirmed by minimizing the sum of the squares of the positional differences (x and y) of the vectors.

3. Results and Discussion

Prior to the scanning probe investigation, the quality of the azobenzene monolayers was checked by contact angle measurements. The advancing contact angle of $89 \pm 1^\circ$ together with the small hysteresis ($\Delta(\cos \theta_r - \cos \theta_a) = 0.17$) measured with water are consistent with well-ordered monolayers exposing aromatic groups at the surface. The STM image, Figure 1A, shows a regular lattice extending over several gold terraces without distortion even across the gold steps (arrows). All protrusions are at the same height level, and no superstructure can be discerned as for dodecanethiol monolayers. The Fourier transform in Figure 1B reveals a nearly rectangular lattice (white lines) with the dimensions $a = 0.63 \pm 0.05$ nm and $b = 0.75 \pm 0.06$ nm and angles $\varphi = 83 \pm 6^\circ$. The regular lattice composing the molecular domain in Figure 1 is surrounded by disordered zones that were usually found to separate two different types of domains as is apparent in the larger AFM scan (Figure 2). Here two types of domains of 10–20 nm in size can be discerned. Domain A (upper left and center of Figure 2) shows the same striped appearance as the STM image in Figure 1 whereas the other domain (domain B) appears more symmetric since it has a center of inversion and equal distances.

Close-up views of domain A (Figure 3A) and domain B (Figure 3B) reveal a rectangular lattice. The striped lattice in domain A is generated by a primitive rectangular unit cell which is confirmed by the Fourier transform of this direct space view (rectangles in Figure 3A,C). The corners of the unit cell are

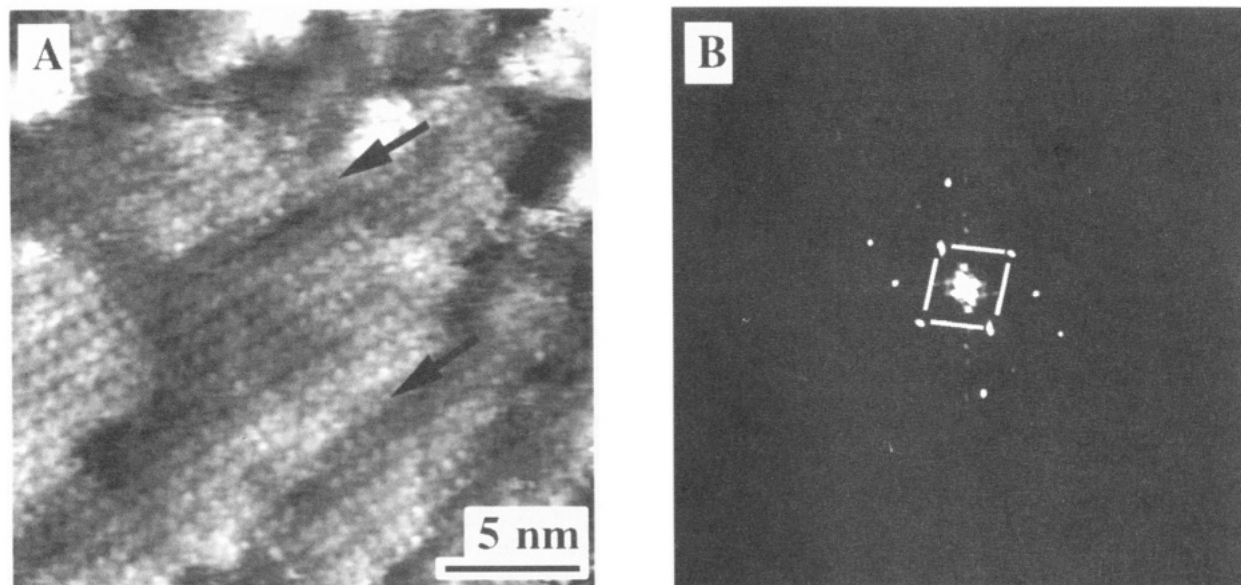


Figure 1. (A) STM constant-current contour obtained with high gap impedance ($I_t = 1.4$ pA, $V_t = 0.86$ V) of 6-[4-(phenylazo)phenoxy]hexane-1-thiol on Au(111). The size of the top view is 20×20 nm², and the contrast from black to white corresponds to 1 nm. A regular lattice covers Au(111) terraces and even extends across gold steps (arrows). (B) Fourier transform with lines linking the reciprocal points of the lattice. The vectors of this lattice are $a = 0.75 \pm 0.06$ nm and $b = 0.63 \pm 0.05$ nm and define an angle of $83 \pm 6^\circ$.

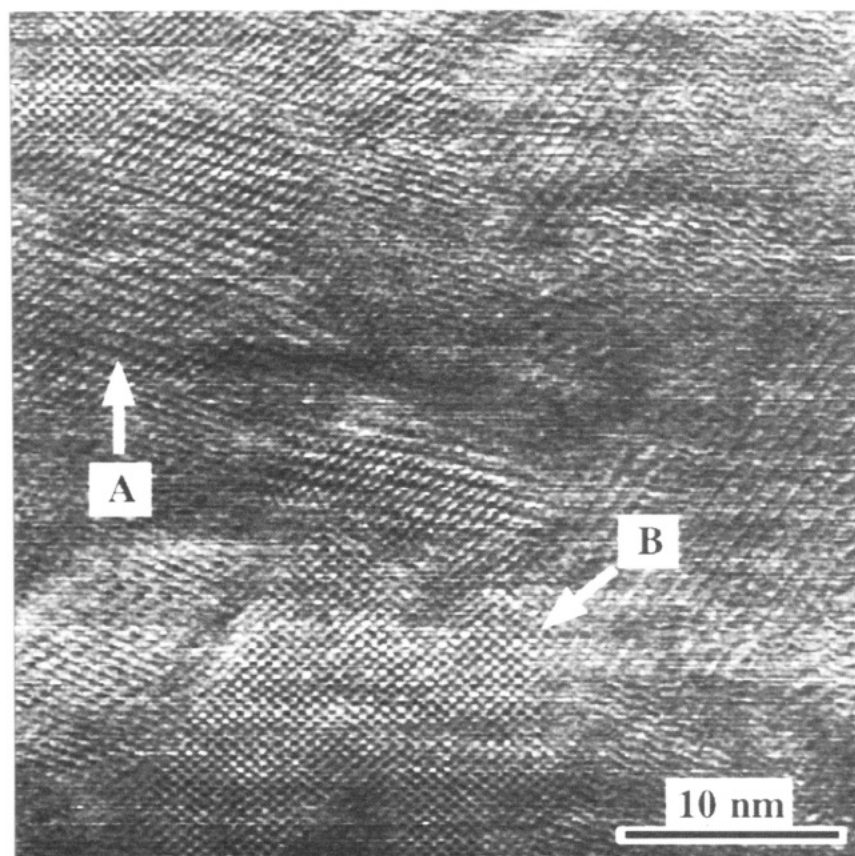


Figure 2. AFM constant-force contour obtained in ethanol at a net force of 3 nN on the same monolayer as in Figure 1. The size of this scan is 40×40 nm². The image shows two types of rectangular lattices (domains A and B) surrounded by disordered zones.

composed of elongated structures, which sometimes show a 2-fold substructure of equal lateral size. The main axes of the elongated structures are parallel to each other and oriented at an angle of 39° with respect to the longer axis (Figure 3A) of the rectangular unit cell. A closer evaluation of domain B and its Fourier transform (Figure 3B,D) shows that this domain is composed of a centered rectangular lattice (rectangle) the structure of which can be attributed to a single molecule (scheme in Figure 3F).

The elongated structures in Figure 3A are roughly twice the size of those in Figure 3B. This suggests that they are composed

of two closely associated molecules. In fact a transition from the centered lattice shown in Figure 3F to the primitive lattice sketched in Figure 3E is possible by approaching center molecules to corner molecules (arrows in Figure 3F). The lateral dimensions of the unit cell are the same for both domains, which is confirmed by the mean ($n = 74$) Fourier transform of many domains: $a = 0.61 \pm 0.04$ nm, $b = 0.79 \pm 0.04$ nm, and φ is $89.9 \pm 3.3^\circ$. (Errors are the standard deviation for a single measurement. They reflect how much the result of a single measurement varied between images; it is not the statistical error of the mean.) They are consistent within experimental errors

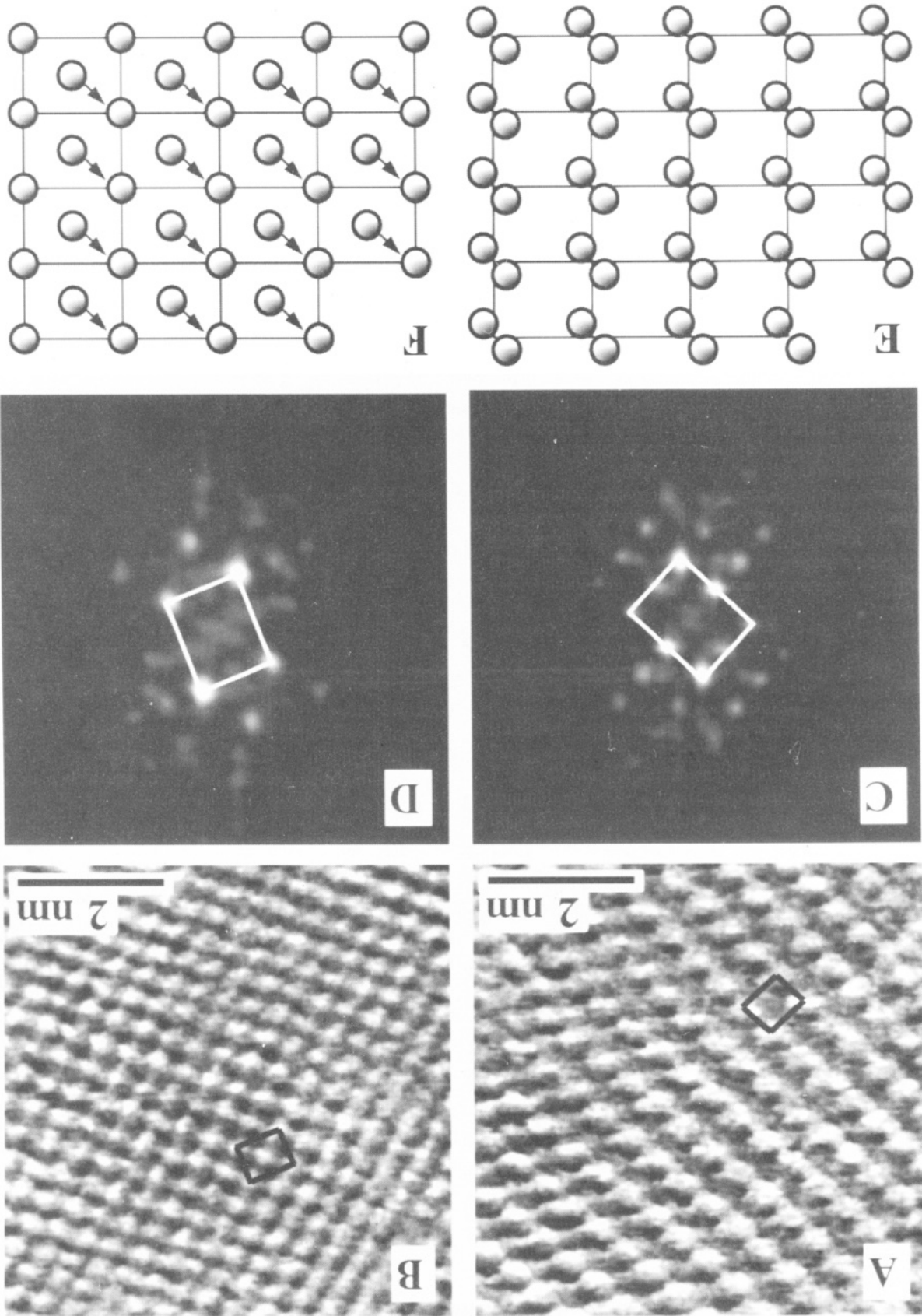


Figure 3. (A,B) Enlarged AFM scans of domains A and B in Figure 2; lateral size $6 \times 6 \text{ nm}^2$. (A) Paired structures define a primitive rectangular cell. (B) Individual structures generate a centered rectangular cell. (C,D) Fourier transforms of panels A and B showing equal unit mesh vectors having the dimensions $a = 0.61 \pm 0.04 \text{ nm}$ and $b = 0.79 \pm 0.04 \text{ nm}$ and an angle of $89.9 \pm 3.3^\circ$. (E,F) Schemes showing the positions of the molecules within the lattices A and B, respectively. Arrows indicate the simple transformation from lattice B to A.

with values found for STM scans. The slightly smaller angle in STM scans is attributed to larger drifts due to the low scan frequency. The unit cell area is $0.48 \pm 0.04 \text{ nm}^2$ for the AFM and $0.47 \pm 0.04 \text{ nm}^2$ for the STM results. For just one azobenzene molecule per unit cell the area would be 2.2 times bigger than for one linear alkanethiol in a $(\sqrt{3} \times \sqrt{3})R30^\circ$ lattice. Considering the molecular dimensions of a diazobenzene moiety (Chart 1), such an expansion seems very unlikely. As

both unit cells contain two molecules, the area occupied by one molecule is $0.24 \pm 0.02 \text{ nm}^2$. This area requirement is also confirmed by results from ellipsometry: closely packed alkanethiol chains would occupy an area of 0.216 nm^2 at a tilt angle of 30° .² If, however, the available space in the SAM were 0.48 nm^2 per molecule, the chains should be highly disordered (liquid-like phase), which would decrease the effective thickness of the monolayer. The measured thickness of $2.0 \pm 0.3 \text{ nm}$, which is very close to the expected height of an azobenzene having a fully extended chain (Chart 1), is thus incompatible with a unit cell of 0.48 nm^2 populated by only one molecule. The measured area is then 1.1 times larger than the molecular area found in linear alkanethiol monolayers.

Molecular domains in these alkyl thiol monolayers were typically delimited at gold step edges. In the case of the azobenzene monolayer, the molecular domain extends over step edges without lateral distortion, even though the gold lattice of a lower terrace is shifted with respect to the upper terrace. This indicates that the pattern of the molecular film is not sensitive to structures of the underlying gold, which is also supported by the AFM observation of the same molecular lattice on polycrystalline sputtered gold. If the order in the molecular film were dominated by the sulfur-gold interaction, no regular lattice should be visible on polycrystalline samples. The rectangular lattice and the incommensurability with the underlying gold and known alkyl lattices imply that the experimentally observed structures are governed by properties of the aromatic azobenzene moiety.

In fact, a comparison with known crystal structures of polynuclear aromatic hydrocarbons shows that interactions between aromatic molecules can form very stable crystals. Although no crystalline structure has been measured so far for the molecule used in this study, it is generally accepted that aromatic molecules adopt only a few typical classes of lattices.³¹ The most abundant crystal packing is the "herringbone" structure, in which the nearest neighbors are nonparallel. A second possible structure is the "sandwich herringbone" packing, in which pairs of parallel rings are nonparallel to the closest neighboring pairs. A third and a fourth type of structure based on interactions between laterally shifted stacks of molecules and graphite-like structures are less frequently found. Linear-fused benzene rings such as naphthalene and tetracene usually adopt the simple herringbone structure (viewed along their main axis), which is also the structure we suggest for azobenzenes.

A film where the molecular interaction dominates over the film-substrate interaction is quite similar to an LB film. In fact there are results on azobenzene-containing LB films^{38,39} which show that the inclusion of an azobenzene moiety into linear alkanic acids increases the molecular area at a given pressure. An exact comparison of the ratio is not possible, however, because the subphase has a significant effect on the molecular areas. Studies of azobenzene-containing LB films indicate that azobenzene moieties supported by an alkyl chain are arranged with their main axes perpendicular to the plane of the layer.^{38,39} In the case of an ω -functionalized SAM, this could mean that the edge of the upper phenyl ring is exposed to the surface.

In fact, the high-resolution studies shown in Figure 4 reveal that the elongated structures are sometimes composed of two elliptical objects with dimensions of $0.24 \times 0.39 \text{ nm}^2$. In the upper right part of the image, two adjacent objects are separated by $0.37 \pm 0.03 \text{ nm}$, and they differ in height by 0.01 nm . The longer axes of the two ellipses are sometimes almost parallel or can have a small angle as shown in model II. The dimers occupy the corners of the rectangular lattice found in Figure 3A,B. This means that these dimers behave as single units for

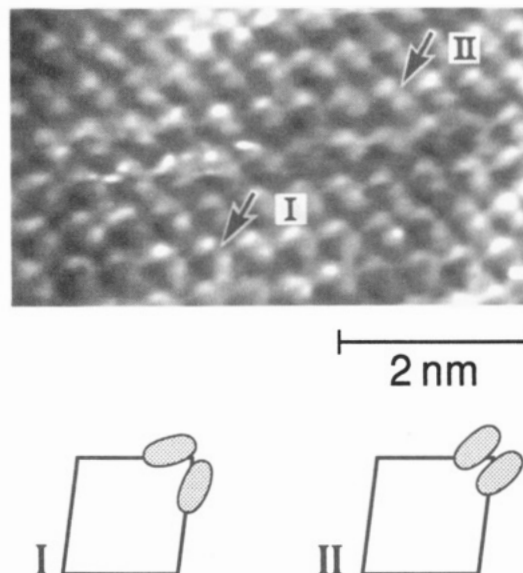


Figure 4. Enlarged view of the same surface as in Figure 1. The STM constant-current contour was obtained at $I_t = 1.3 \text{ pA}$ and $V_t = 0.98 \text{ V}$. The size of the top view is $5 \times 3 \text{ nm}^2$, and the contrast from black to white is 0.06 nm . Protrusions composed of pairs of elliptical objects with dimensions of $0.24 \times 0.39 \text{ nm}^2$ define a nearly rectangular lattice. Each object corresponds to the upper edge of a phenyl ring. The rings either form an angle (I) or are parallel within a dimer (II).

operation in the reciprocal space, i.e., the principal vectors of the Fourier transform also define a rectangle. In the lower left part of Figure 4, two elliptical objects with the same dimensions and height difference as above form an angle of approximately 40° (model I). The angle between the two ellipses is not fixed but can vary within the limits given by models I and II.

Aromatic systems can be described as a positively charged σ -framework sandwiched between the two negative π -electron clouds.⁴⁰ The interaction between two face-to-face π -systems is repulsive, but becomes attractive when the π -systems glide along each other or rotate away from each other. The combination of the angle of rotation and the in-plane offset (gliding) yields a large number of isoenergetic geometrical arrangements. This is in accordance with the observation of a variable angle between aromatic rings in the high-resolution scan in Figure 4. The molecules are restricted in their vertical position, but the other degrees of freedom (lateral shift and rotation) lead to a variety of patterns found in this figure. The AFM Figures 2 and 3 are recorded in the friction mode. Although this mode turned out to be very useful to image lattices on the molecular scale, the contrast mechanism is not well understood. Thus from the present data we cannot decide if AFM can or cannot provide information on the orientation of the molecular orbitals. By STM, the molecule contour appears as an elongated anisotropic structure since STM resolves the electronic contributions from the probed molecule^{41,42} and thus reveals the relative orientation of the phenyl rings present at the termina of the monolayer. Another striking result is the coexistence of domains with two different stable lattices. Calculations show that, within the lattice classes, a large variety of possible geometries exists between aromatic molecules that lead to several packing structures, close in energy, separated by interconversion energy barriers.⁴⁰ As the domains grow at the beginning of adsorption, interconversion between each structure becomes unlikely at room temperature.

The pattern generated by the phenyl rings (Figure 3) optimizes the amount of attractive interaction between the two aromatic systems. If the rectangular lattices observed at the monolayer surface are translated to the head groups, the sulfur lattices would be incommensurate with the gold substrate and would

have to overcome the difference in energy between top and hollow sites. Another possibility is that the alkyl chains mediate a transition between the lattice observed for the tail group and a different lattice of the sulfur head groups, where these sulfurs occupy 3-fold hollow sites.⁴³

This second hypothesis is supported by a recent MD study of perfluoroalkylmercaptans on Au(111): Röthlisberger et al. found that interaction between the bulky perfluoroalkyl chains caused these chains to order incommensurately with the substrate, where the sulfurs nevertheless occupy 3-fold hollow sites. So far, no experimental data is available on the corrugation of the adsorption energy potential on gold. The corrugation is estimated to be of the order of 8 kcal/mol,⁴⁴ which corresponds to 30% of 28 kcal/mol, the total chemisorption energy.¹² Experimental results for the interaction energies of aromatic systems are scarce and available for only a few model systems. In the case of azobenzene, however, the aromatic interaction dominates over the alkyl interaction and perhaps the gold surface energy corrugation.

4. Conclusion

This study addresses order at the outer surface of a monolayer on gold and shows that anisotropic space requirements and interactions of azobenzene groups can dominate the order in a SAM and force molecules into lattices that are incommensurate with the underlying Au(111). Whether the sulfur lattice in this monolayer is commensurate with Au(111) remains unresolved since the alkyl chains provide a geometrical buffer between order in the end groups and order in the head groups. We identify two types of lattices at the monolayer surface: a centered lattice, which we ascribe to a "herringbone" pattern of the aromatic moieties, and a primitive lattice in which the corners of the unit cell are populated with pairs like in the "sandwich herringbone" structure. The first lattice has quite fixed geometrical constraints, whereas in the second lattice, various isoenergetic configurations of phenyls with *x,y* translations and rotations are possible. Mixtures of molecules having different tail groups can form new structures. Such systems can be used to study the balance between various contributions and also to study lateral molecular diffusion. This is the scope of questions that will be addressed in a subsequent paper.⁴⁵

The phenyl ring upper edges appear in the STM as elongated elliptical objects. This seems to be a systematic difference due to the different physical properties that are detected by the two instruments. In the present case AFM detects a friction contour at constant force whereas STM images electronic distributions. Comparison of the two data sets distinguishes the friction contour from the molecular orbital distribution. This difference seems to be most pronounced for aromatic systems with extended delocalized π -orbitals. Because the images have been recorded with different instrumental setups, this analysis remains somewhat speculative. But what becomes clear is that combinations of both STM and AFM instruments can provide much more information on a given sample than each method alone.⁴⁶

Acknowledgment. We would like to thank H. Biebuyck, M. Klein, H. Sigrist, and M. Sprik for helpful discussions. E.D. acknowledges financial support from the Swiss National Foundation Project 24+, B.M. acknowledges partial funding by the BBW Switzerland within the ESPRIT basic research project PRONANO (8523). H.K. thanks the Ministry of Education of Korea for financial support, and H.W. and H.R. thank DFG Germany. T.T. thanks T. Uchiyama from the Advanced Technology Institute for financial support. M.J., H.-J.B., and E.B. thank the DFG SPP "Neue Mikroskopische Techniken für Biologie und Medizin" for financial support and H. Volk for her help with the photographs.

References and Notes

- (1) Swalen, J. D.; Allara, D. L.; Andrade, J. D.; Chandross, E. A.; Garoff, S.; Israelachvili, J.; McCarthy, T.-J.; Murray, R.; Pease, R. F.; Rabolt, J. F.; Wynne, K. J.; Yu, H. *Langmuir* **1987**, *3*, 932.
- (2) Ulman, A. *An Introduction to Ultrathin Films*; Academic Press: San Diego, CA, 1991.
- (3) Dubois, L. H.; Nuzzo, R. G. *Annu. Rev. Phys. Chem.* **1992**, *43*, 437.
- (4) Kumar, A.; Biebuyck, H. A.; Whitesides, G. M. *Langmuir* **1994**, *10*, 1498.
- (5) Sagiv, J. *J. Am. Chem. Soc.* **1980**, *102*, 92.
- (6) Laibinis, P. E.; Whitesides, G. M.; Allara, D. L.; Tao, Y.-T.; Parikh, A. N.; Nuzzo, R. G. *J. Am. Chem. Soc.* **1991**, *113*, 7152.
- (7) Wasserman, S. R.; Tao, Y.-T.; Whitesides, G. M. *Langmuir* **1989**, *5*, 1074.
- (8) Ulman, A. *Angew. Chem. Adv. Mater.* **1990**, *2*, 573.
- (9) Laibinis, P. E.; Hickman, J. J.; Wrighton, M. S.; Whitesides, G. M. *Science* **1989**, *245*, 845.
- (10) Porter, M. D.; Bright, T. B.; Allara, D. L.; Chidsey, C. E. D. *J. Am. Chem. Soc.* **1987**, *109*, 3559.
- (11) Bain, C. D.; Whitesides, G. M. *Angew. Chem., Int. Ed. Engl.* **1989**, *28*, 506.
- (12) Nuzzo, R. G.; Dubois, L. H.; Allara, D. L. *J. Am. Chem. Soc.* **1990**, *112*, 558.
- (13) Whitesides, G. M.; Bain, C. D.; Evall, J. *J. Am. Chem. Soc.* **1989**, *111*, 7155.
- (14) Häußling, L.; Michel, B.; Ringsdorf, H.; Rohrer, H. *Angew. Chem., Int. Ed. Engl.* **1991**, *30*, 569.
- (15) Häußling, L.; Ringsdorf, H.; Schmitt, F.-J.; Knoll, W. *Langmuir* **1991**, *7*, 1837.
- (16) Lee, H.; Kepley, L. J.; Hong, H.-G.; Akhter, S.; Mallouk, T. E. *J. Phys. Chem.* **1988**, *92*, 2597.
- (17) Alves, C. A.; Smith, E. L.; Porter, M. D. *J. Am. Chem. Soc.* **1992**, *114*, 1222.
- (18) Pan, J.; Tao, N.; Lindsay, S. M. *Langmuir* **1993**, *9*, 1556.
- (19) Butt, H.-J.; Seifert, K.; Bamberg, E. *J. Phys. Chem.* **1993**, *97*, 7316.
- (20) Widrig, C. A.; Alves, C. A.; Porter, M. D. *J. Am. Chem. Soc.* **1991**, *113*, 2805.
- (21) Kim, Y.-T.; Bard, A. J. *Langmuir* **1992**, *8*, 1096.
- (22) Kim, Y.-T.; McCauley, R. L.; Bard, A. J. *J. Phys. Chem.* **1992**, *96*, 7416.
- (23) Schönenberger, C.; Sondag-Hüthorst, J. A. M.; Jorritsima, J.; Fokkink, L. G. J. *Langmuir* **1994**, *10*, 611.
- (24) Delamarche, E.; Michel, B.; Gerber, Ch.; Anselmetti, D.; Güntherodt, H.-J.; Wolf, H.; Ringsdorf, H. *Langmuir* **1994**, *10*, 2869.
- (25) Poirier, G. E.; Tarlov, M. J. *Langmuir*, **1994**, *10*, 2853.
- (26) Camillone, N., III; Eisenberger, P.; Leung, B. T. Y.; Schwartz, P.; Scoles, G.; Poirier, G. E.; Tarlov, M. J. *J. Chem. Phys.* **1994**, *101*, 11031.
- (27) Delamarche, E.; Michel, B.; Kang, H.; Gerber, Ch. *Langmuir* **1994**, *10*, 4103.
- (28) Shnidman, Y.; Ulman, A.; Eilers, J. E. *Langmuir* **1993**, *9*, 1071.
- (29) Evans, S. D.; Urankar, E.; Ulman, A.; Ferris, N. *J. Am. Chem. Soc.* **1991**, *113*, 4121.
- (30) Chang, S.-C.; Chai, I.; Tao, T.-T. *J. Am. Chem. Soc.* **1994**, *116*, 6792.
- (31) Desiraju, G. R.; Gavezzotti, A. *J. Chem. Soc., Chem. Commun.* **1989**, 621.
- (32) Overney, R. M.; Howald, L.; Frommer, J.; Meyer, E.; Brodbeck, D.; Güntherodt, H.-J. *Ultramicroscopy* **1992**, *42-44*, 983.
- (33) Chidsey, C. E. D.; Loiacono, D. N.; Sleator, T.; Nakahara, S. *Surf. Sci.* **1988**, *200*, 45.
- (34) Bucher, J.-P.; Santesson, L.; Kern, K. *Langmuir* **1994**, *10*, 979.
- (35) Wasserman, S. R.; Whitesides, G. M.; Tidswell, I. M.; Ocko, B. M.; Pershan, P. S.; Axe, J. D. *J. Am. Chem. Soc.* **1989**, *111*, 5852.
- (36) Bain, C. D.; Troughton, E. B.; Tao, Y.-T.; Evall, J.; Whitesides, G. M.; Nuzzo, R. G. *J. Am. Chem. Soc.* **1989**, *111*, 321.
- (37) Michel, B.; Novotny, L.; Dürig, U. *Ultramicroscopy* **1992**, *42-44*, 1647.
- (38) Albrecht, O.; Cumming, W.; Kreuder, W.; Laschewsky, A.; Ringsdorf, H. *Colloid Polym. Sci.* **1986**, *264*, 659.
- (39) Sato, T.; Ozaki, Y.; Iriyama, K. *Langmuir* **1994**, *10*, 2363.
- (40) Hunter, C. A.; Sanders, J. K. M. *J. Am. Chem. Soc.* **1990**, *112*, 5525.
- (41) Sautet, P.; Joachim, C. *Chem. Phys. Lett.* **1991**, *185*, 23.
- (42) Weiss, P. S.; Eigler, D. M. *Phys. Rev. Lett.* **1993**, *71*, 3139.
- (43) Röthlisberger, U.; Klein, M. L.; Sprik, M. *J. Mater. Chem.* **1994**, *4*, 793.
- (44) Mar, W.; Klein, M. L. *Langmuir* **1994**, *10*, 188.
- (45) Takami, T.; Delamarche, E.; Michel, B.; Gerber, Ch.; Wolf, H.; Ringsdorf, H. *Langmuir*, submitted.
- (46) Kelty, S. P.; Ruppert, A. F.; Chianelli, R. R.; Ren, J.; Whangbo, M.-H. *J. Am. Chem. Soc.* **1994**, *116*, 7857.